Optical properties of $Al_xGa_{1-x}As$

Cite as: Journal of Applied Physics **60**, 754 (1986); https://doi.org/10.1063/1.337426
Submitted: 05 December 1985 • Accepted: 28 March 1986 • Published Online: 04 June 1998

D. E. Aspnes, S. M. Kelso, R. A. Logan, et al.

Optical properties of $Al_xGa_{1-x}As$

D. E. Aspnes
Bell Communications Research, Inc., Murray Hill, New Jersey 07974

S. M. Kelso
Xerox Palo Alto Research Center, Palo Alto, California 94304

R. A. Logan
AT&T Bell Laboratories, Murray Hill, New Jersey 07974

R. Bhat
Bell Communications Research, Inc., Murray Hill, New Jersey 07974

(Received 5 December 1985; accepted 28 March 1986)

We report pseudodielectric function $\langle\epsilon\rangle$ data for $Al_xGa_{1-x}As$ alloys of target compositions $x = 0.00$–0.80 in steps of 0.10 grown by liquid-phase epitaxy and measured by spectroellipsometry. Cleaning procedures that produce abrupt interfaces between the technologically relevant alloys $x \leqslant 0.5$ and the ambient are described. The $\langle\epsilon_2\rangle$ data are corrected near the fundamental direct absorption edge by a Kramers–Kronig analysis of the $\langle\epsilon_1\rangle$ data to circumvent a limitation of the rotating-analyzer ellipsometric technique. The results and the associated pseudo-optical functions $\langle n\rangle$, $\langle R\rangle$, and $\langle\alpha\rangle$ are listed in tabular form. Accurate values of the E_0 and E_1 threshold energies are determined from these spectra by Fourier methods. From these values, and from similar values for a GaAs-capped AlAs sample grown by organometallic chemical vapor deposition, the dependencies of the E_0 and E_1 interband critical point energies on nominal composition are obtained. Cubic polynomial representations of these dependencies are determined to allow nominal Al fractions to be calculated analytically from optical threshold data. The systematic behavior of $\langle\epsilon_1\rangle$ at 1.5 eV and of the E_2 peak in $\langle\epsilon_2\rangle$ near 5 eV show that scatter in these data is less than 1% of the peak values of the spectra for $x \leqslant 0.5$. For $x \geqslant 0.6$ the peak data appear to show systematic discrepancies indicating that chemical cleaning cannot completely remove surface overlayers on high-Al-content samples. Optical measurements for a sample with $x = 0.9$ also reveal that the oxidation of high-Al samples proceeds irregularly and not along a uniform spatial front. Interpolation procedures to obtain approximate representations of dielectric function spectra at compositions other than those measured are discussed, and suggestions for improving accuracy in future optical measurements on these and related materials are also given.

I. INTRODUCTION

The materials in the binary alloy series $Al_xGa_{1-x}As$ are essentially lattice matched over the entire composition range. This attribute has been of considerable technical importance, because it has made possible the growth of artificial structures with electronic energy levels tailored to a wide variety of fundamental and applied purposes.[1–5] These structures and their interfaces can be characterized conveniently and nondestructively by visible-near UV optical reflection techniques.[6–12] However, these techniques require an accurate data base, but at present only incomplete dielectric function data are available.[7–9,12–16]

Here, we report room-temperature pseudodielectric $\langle\epsilon\rangle$ and related optical function data for $Al_xGa_{1-x}As$ alloys for energies E from 1.5 to 6.0 eV and for compositions x from 0.00 to 0.80 in steps of approximately 0.10. The scatter in $\langle\epsilon\rangle$ values at selected wavelengths in the technologically relevant composition range $x \leqslant 0.5$ is less than 1% of the peak ϵ value, and we estimate the data in this range to be accurate on the same scale to within 2%. Our results not only provide the data base needed for nondestructive optical analysis, but also yield information about the compositional dependencies of various parameters, such as critical point threshold energies, that can improve our understanding of the fundamental physical properties of these materials. In addition, the cleaning and stripping procedures developed to obtain these data should be generally useful. Finally, oxidation results for a sample with $x = 0.90$ reveal that at high relative Al concentrations oxidation proceeds via local penetration rather than along a uniform front, so that the semiconductor–oxide interface of such material is more appropriately described as a physical mixture of oxide and alloy.

II. SAMPLE GROWTH, SAMPLE PREPARATION, AND OPTICAL MEASUREMENTS

$Al_xGa_{1-x}As$ layers of the order of 2–3 μm thick were grown by liquid-phase epitaxy (LPE) on semi-insulating Cr-doped GaAs substrates of ⟨100⟩ surface orientation. Target compositions were $x = 0.00$ to 0.90 in steps of 0.10. Following growth, the surfaces of the $Al_xGa_{1-x}As$ layers were electrochemically anodized to thicknesses of the order of 50–100 nm to protect the material from attack by the ambient. Due to the importance of energy threshold data for the binary endpoint AlAs, a sample of this material grown by organometallic chemical vapor deposition (OMCVD) and capped with a protective GaAs overlayer approximately

 0021-8979/86/140754-14$02.40

50 Å thick was also analyzed. However, AlAs thickness variations limited useful results on this sample to the E_1 critical point energy and to approximate estimates of the height of the E_2 peak in ϵ_2.

Owing to the strong dependence of the Al composition of the film on the Al fraction in the melt,[17] especially for low Al concentrations, exact control of the Al composition is difficult to achieve. However, Auger analysis on similar samples has shown that typical differences between actual and target compositions do not exceed 0.03.[18] As discussed below, the more precise composition estimates that we obtain from threshold energies of the E_0 and E_1 critical point structures in the optical spectra support this conclusion: scatter in the actual compositions do not differ from mean values by more than 0.02.

Optical data were taken with an automatic rotating-analyzer spectroellipsometer described elsewhere.[19] The effect of the optical activity of the quartz Rochon prisms on the data was taken into account by standard equations.[20]

Preparation procedures for optical measurements were similar to those previously used to obtain accurate dielectric function data for Si, Ge, and the major III-V compound semiconductors.[21,22] An initial set of data was taken on each as-grown sample by mounting it on a vacuum chuck in a windowless cell, optically prealigning it, stripping it of its protective oxide and other surface films with KOH in water, and then maintaining it in a dry N_2 atmosphere to keep its surface in the as-prepared condition. Surface quality was assessed in the usual manner by tuning the monochromator to the wavelength of the E_2 peak in ϵ_2 and processing the sample until the imaginary part $\langle\epsilon_2\rangle$ of the pseudodielectric function $\langle\epsilon\rangle$ had reached its maximum value.[23] The KOH concentration initially used was 1 N (*p*H 14), for which the ⟨100⟩ GaAs surface is stable.[24] However, 1 N KOH was found to microscopically roughen alloys with $x \geqslant 0.35$ because of the extreme reactivity of Al in strongly basic solutions. For these alloys, some success was achieved by progressively diluting the KOH solutions with water as the oxide thickness approached zero. But this procedure was awkward, as it required continuous monitoring of the stripping process with the spectroellipsometer. And since the magnitude of the E_2 peak in $\langle\epsilon_2\rangle$ was not known *a priori*, the optimal point at which to stop processing was not determined until after it had passed.

For this reason, a second set of data was taken at a later time by polishing the stripped samples with Br_2-methanol solutions, optically prealigning them in the windowless cell, and then rinsing them with various stripping solutions. Again, the cleaning procedures were monitored with the spectroellipsometer. Not surprisingly, the optimal approach varied with Al composition, with the alloys of higher Al fractions requiring more dilute processing solutions. In every case the relatively sharp E_0 critical point structures in $\langle\epsilon_1\rangle$ and the heights of the E_2 peaks in $\langle\epsilon_2\rangle$ were found to be improved with respect to the corresponding features measured in the first investigation. After it became apparent that further processing would lead to no further improvement, $\langle\epsilon\rangle$ data were acquired for the record. The procedures and solutions used to obtain these latter data are summarized in Table I.

The ellipsometer yields data as $(\tan\psi, \cos\Delta)$, where $(\tan\psi)$ and Δ are the amplitude and phase, respectively, of the complex reflectance ratio. The pseudodielectric function is a derived quantity obtained from these data by means of the two-phase (substrate-ambient) model.[25] The pseudodielectric function would be exactly equal to the true bulk dielectric function of a given sample if its surface were perfectly abrupt and film-free. Because these ideal conditions are never achieved in practice, $\langle\epsilon\rangle$ is necessarily an approximation to the true bulk dielectric function of a given material. However, experience has shown that the most consistent and reproducible dielectric function data, i.e., those most nearly independent of both experimental technique and experimentalist, are those where attention is given to carefully preparing samples with the best possible surfaces rather than to carefully compensating the data for the presence of removable overlayers.[26] Because neither the thickness nor the dielectric properties of the residual surface layer(s) are known, we do not attempt any corrections for them but present our results directly in pseudodielectric function form.

TABLE I. Compositions of the polishing and stripping solutions used to prepare abrupt interfaces on ⟨100⟩ $Al_xGa_{1-x}As$ samples for the target compositions indicated. Exact concentrations are not critical. After stripping native oxides with a 1:1 solution of NH_4OH in water, the samples were chemomechanically polished on lens paper for 1 min using the solutions given, after which the solutions were quenched to pure methanol. The stripping solutions indicated were flowed for 3 s over the optically prealigned samples, rinsed off with the appropriate diluent (methanol for Br_2, water for NH_4OH), and blown dry with dry N_2 between solutions. Stripping sequences were methanol: Br_2 in methanol (methanol rinse); water: NH_4OH in water (water rinse). The final treatment is indicated in the last column. For $0.4 < x < 0.6$, the stripping sequence was terminated with NH_4OH *without* the water rinse. For $x = 0.8$, the water step was eliminated entirely. Sequences were repeated at least twice to ensure that observed E_2 peak values had reached a limit.

Target composition	Br_2 in methanol (polishing)	Br_2 in methanol (stripping)	NH_4OH in water (stripping)	Final rinse
$x = 0.00$	0.05 vol %	0.02 vol %	50 vol %	water
0.10	0.01	0.01	50	water
0.20	0.01	0.01	50	water
0.30	0.01	0.01	50	water
0.40	0.01	0.01	50	NH_4OH
0.50	0.01	0.01	10	NH_4OH
0.60	0.01	0.01	10	NH_4OH
0.70	0.01	0.01	10	Br_2-meth.
0.80	0.002	0.002	10	Br_2-meth.

III. RESULTS AND DISCUSSION

A. Spectra

Pseudodielectric function spectra from 1.5 to 6.0 eV for the nine alloys studied in detail here are shown in Figs. 1 and 2. The $\langle\epsilon\rangle$ data and the associated derived pseudoquantities, the complex pseudorefractive index

$$\langle\tilde{n}\rangle = \langle n\rangle + i\langle k\rangle = \langle\epsilon\rangle^{1/2},$$

the pseudoabsorption coefficient $\langle\alpha\rangle = 4\pi\langle k\rangle/\lambda$, and the normal-incidence pseudoreflectance

$$\langle R\rangle = [(\langle n\rangle - 1)^2 + \langle k\rangle^2]/[(\langle n\rangle + 1)^2 + \langle k\rangle^2]$$

are given in Tables II through X.[27] Because the data for the binary endpoint GaAs was within experimental uncertainty of that previously published for this material,[22] the data for GaAs are simply repeated from Ref. 22 with a Kramers–Kronig correction applied to the first five values of $\langle\epsilon_2\rangle$ and associated quantities, as discussed below.

For each material, these spectra are reported as-measured at energies higher than about 0.2 eV above the E_0 transition. However, the results are modified at lower energies to compensate for artifacts caused by limitations of the sample geometry and the measurement technique. Thin film samples whose thickness is of the order of the wavelength of light produce interference oscillations in optical data in the region of film transparency due to multiple internal reflections within the film. The magnitudes of the oscillations observed in our measurements were less than 30% of those expected on the basis of model calculations assuming that the layers were homogeneous and uniformly thick. We attribute this attenuation to the ~1500-Å compositional gradient that is known to occur at the GaAs–alloy interface in LPE films.[28] This gradient would be expected to smooth the discontinuity between the substrate and the film and thereby reduce the amplitude of the back-reflected component.

Under these circumstances, attempts to interpret the data in terms of the three-phase (substrate–film–ambient) model[25] cannot succeed, as the reduced amplitude of the interference oscillations would be incorrectly interpreted within the model as an unphysically close match between the dielectric function of the film and that of the substrate. But eliminating the interference oscillations by suitably grading the substrate–film interface is functionally equivalent to eliminating them by absorbing them in the film, as is easily shown from the explicit equations. Consequently, in the absence of interference oscillations the film pseudodielectric functions would be given directly by the two-phase model whether the oscillations were suppressed by grading or by absorption. If residual oscillations are present, it can be shown to first order in the oscillation amplitude that the film pseudodielectric function is just given by the average value. Accordingly, we have corrected $\langle\epsilon_1\rangle$ in the spectral region below E_0 by simply replacing them with the local average values. The oscillations for the sample with $x = 0.80$ were large and apparently outside the region of validity of the first-order expansion. The data for this sample had to be treated differently, as discussed below.

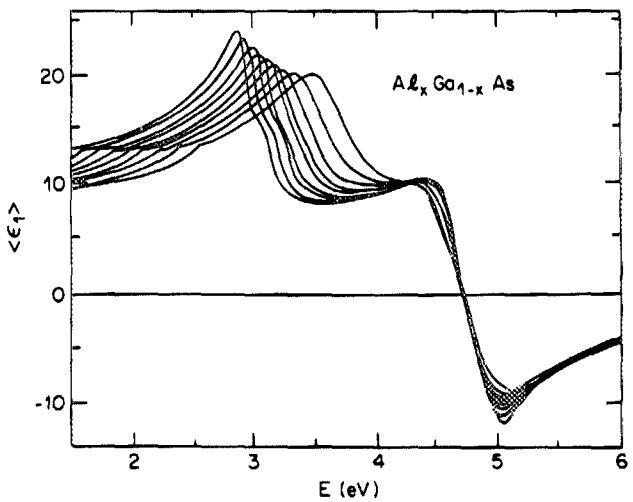

FIG. 1. Real part $\langle\epsilon_1\rangle$ of the pseudodielectric function for the nine compositions studied here, from left to right with increasing x.

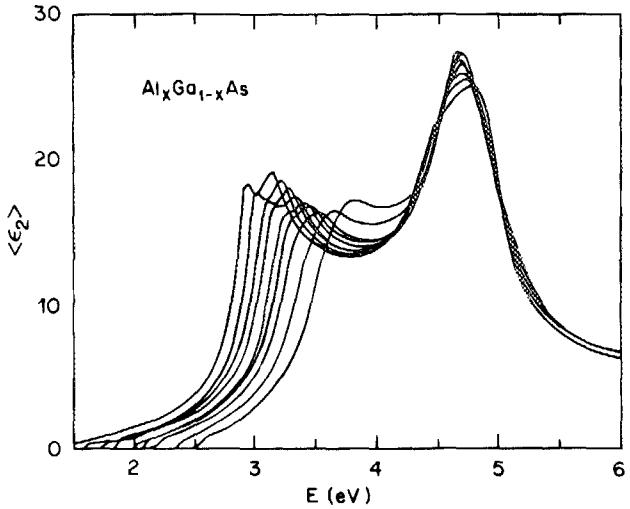

FIG. 2. As Fig. 1, but for $\langle\epsilon_2\rangle$.

The results for $\langle\epsilon_2\rangle$ in this spectral range were also modified to compensate for the inability of rotating-analyzer ellipsometers to accurately measure small values of $\langle\epsilon_2\rangle$. This limitation does not cause any practical difficulties below the fundamental edges of the direct-band-gap alloys, where the material is transparent and the inaccurate $\langle\epsilon_2\rangle$ values can simply be replaced by zero. But for alloys with compositions $x \geq 0.45$ the fundamental absorption edge is indirect.[29] Since the grading of the back layer prevented us from performing the usual three-phase-model inversion, we had no way of determining ϵ_2 in the indirect absorption region. For optical modeling purposes the difference between "small" and zero is generally negligible, so we again replaced the inaccurate values with zero. But for applications where the indirect absorption, though weak, is important, this limitation must be kept in mind.

For the small values of $\langle\epsilon_2\rangle$ in the vicinity of the E_0 transition itself, we calculated the Kramers–Kronig transformation of the corresponding structure in $\langle\epsilon_1\rangle$ and then merged this structure with the original data about 0.1–0.2 eV above the E_0 threshold energy. The actual Kramers–Kronig calculations were done using Fourier methods to conveniently separate information from noise and to avoid distor-

TABLE II. Pseudo-optical functions of $Al_xGa_{1-x}As$: composition $x = 0.00$ (GaAs).

Energy	$\langle\epsilon_1\rangle$	$\langle\epsilon_2\rangle$	$\langle n\rangle$	$\langle k\rangle$	$\langle R\rangle$	$10^{-3}\langle\alpha\rangle$ (cm^{-1})
1.500	13.435	0.436	3.666	0.059	0.327	9.03
1.600	13.683	0.687	3.700	0.093	0.330	15.06
1.700	13.991	0.922	3.742	0.123	0.335	21.22
1.800	14.307	1.192	3.786	0.157	0.340	28.72
1.900	14.607	1.367	3.826	0.179	0.344	34.40
2.000	14.991	1.637	3.878	0.211	0.349	42.79
2.100	15.463	1.893	3.940	0.240	0.356	51.15
2.200	16.031	2.212	4.013	0.276	0.363	61.46
2.300	16.709	2.622	4.100	0.320	0.372	74.56
2.400	17.547	3.123	4.205	0.371	0.382	90.34
2.500	18.579	3.821	4.333	0.441	0.395	111.74
2.600	19.885	4.841	4.492	0.539	0.410	142.02
2.700	21.550	6.536	4.694	0.696	0.429	190.53
2.800	23.605	9.830	4.959	0.991	0.456	281.33
2.900	22.558	17.383	5.052	1.721	0.490	505.75
3.000	16.536	17.571	4.509	1.948	0.472	592.48
3.100	14.519	18.765	4.373	2.146	0.477	674.17
3.200	10.271	18.022	3.938	2.288	0.468	742.21
3.300	9.086	16.037	3.709	2.162	0.447	723.09
3.400	8.626	14.929	3.596	2.076	0.434	715.28
3.500	8.413	14.216	3.531	2.013	0.425	714.20
3.600	8.355	13.739	3.495	1.965	0.419	717.14
3.700	8.419	13.459	3.485	1.931	0.415	724.14
3.800	8.611	13.365	3.501	1.909	0.414	735.28
3.900	8.890	13.470	3.538	1.904	0.416	752.62
4.000	9.279	13.832	3.601	1.920	0.421	778.65
4.100	9.754	14.538	3.692	1.969	0.430	818.23
4.200	10.235	15.767	3.810	2.069	0.444	880.86
4.300	10.412	17.803	3.939	2.260	0.466	984.86
4.400	9.545	20.582	4.015	2.563	0.494	1143.26
4.500	6.797	22.845	3.913	2.919	0.521	1331.28
4.600	4.163	23.891	3.769	3.169	0.540	1477.66
4.700	1.030	24.835	3.598	3.452	0.565	1644.29
4.800	− 3.045	25.196	3.342	3.770	0.596	1834.17
4.900	− 8.022	23.394	2.890	4.047	0.633	2009.91
5.000	− 11.514	18.564	2.273	4.084	0.668	2069.81
5.100	− 11.156	13.677	1.802	3.795	0.676	1961.86
5.200	− 9.578	11.143	1.599	3.484	0.661	1836.15
5.300	− 8.350	9.758	1.499	3.255	0.644	1748.74
5.400	− 7.435	8.806	1.430	3.079	0.628	1685.29
5.500	− 6.705	8.123	1.383	2.936	0.613	1636.68
5.600	− 6.107	7.593	1.349	2.815	0.599	1597.99
5.700	− 5.589	7.182	1.325	2.710	0.584	1565.73
5.800	− 5.171	6.882	1.311	2.625	0.571	1543.08
5.900	− 4.876	6.587	1.288	2.557	0.562	1528.86
6.000	− 4.511	6.250	1.264	2.472	0.550	1503.21

tions.[30] The first five data points in $\langle\epsilon_2\rangle$ and in quantities derived from these data differ in Table II from the corresponding points in Table V in Ref. 22 for this reason.

The validity of the above corrections and the self-consistency of the data were checked by calculating the Kramers–Kronig transform of the $\langle\epsilon_2\rangle$ data from 1.5 to 6.0 eV and subtracting the result from the $\langle\epsilon_1\rangle$ data. If the data were completely self-consistent, the difference would show only the smooth variation due to contributions from absorption processes outside the experimentally accessible energy range. Consistency was observed to within 1.4% of the E_2 peak value for all samples except for that with $x = 0.80$, where the measured $\langle\epsilon_1\rangle$ spectrum was found to be low by 0.51 nearly everywhere below the E_0 threshold. *For this composition only* the measured $\langle\epsilon_1\rangle$ spectrum was corrected in this spectral range to bring it into coincidence with the $\langle\epsilon_1\rangle$ spectrum calculated by the Kramers–Kronig transform of $\langle\epsilon_2\rangle$.

Because these artifacts could not be dealt with so directly with LPE material containing 90 to 100% Al, $\langle\epsilon\rangle$ data for these compositions were deemed of insufficient quality to be useful for reference purposes and are not given here. However, the sample of target composition $x = 0.90$ was useful for oxidation studies, as will be discussed below.

B. Compositions

The target compositions were values of x from 0.00 to 1.00 in increments of 0.10. Because these data are intended for reference purposes, it is important that the compositions be determined to a precision better than that possible from growth conditions alone. Accordingly, we determined the

threshold energies of the E_0 transitions of the samples of target compositions $0.10 \leqslant x \leqslant 0.80$, along with two samples of nominal compositions $x = 0.14$ and 0.24 grown by molecular-beam epitaxy (MBE), and then least-squares fit the resulting data to a cubic polynomial whose endpoints $x = 0.00$ and 1.00 were constrained to the known[29] room-temperature threshold energies of 1.424 and 3.018 eV for GaAs and AlAs, respectively. A cubic functional form was used because previous measurements have shown that the variation of the E_0 threshold energy with composition cannot be described over the entire range by a simple quadratic function.[9,14,29]

Because the E_0 peak is sharp and well separated from other structures in the optical spectrum, we determined the critical point energies in reciprocal space by weighting the Fourier coefficients of the E_0 structures according to the first derivative and fitting amplitudes and phases with the appropriate critical point function.[30] By fitting a polynomial to these critical point energies, we are essentially assuming that the target compositions are accurate to within a statistical fluctuation that is averaged out by the least-squares polynomial fit. The best-fit expression itself is found to be

$$E_0(x) = 1.424 + 1.594x + x(1-x)(0.127 - 1.310x)\ \text{eV}. \quad (1)$$

We shall refer to values of x obtained by solving Eq. (1) for x for a given threshold energy E_0 as optically determined compositions.

The results are shown explicitly in Fig. 3. The circles represent the threshold energies determined from our spectra plotted as a function of *target* composition. The triangles show analogous data for the two MBE samples. The dashed curve shows the piecewise linear-quadratic room-temperature relationship given by Casey and Panish.[29] It is clear that the E_0 threshold energies deviate considerably from this

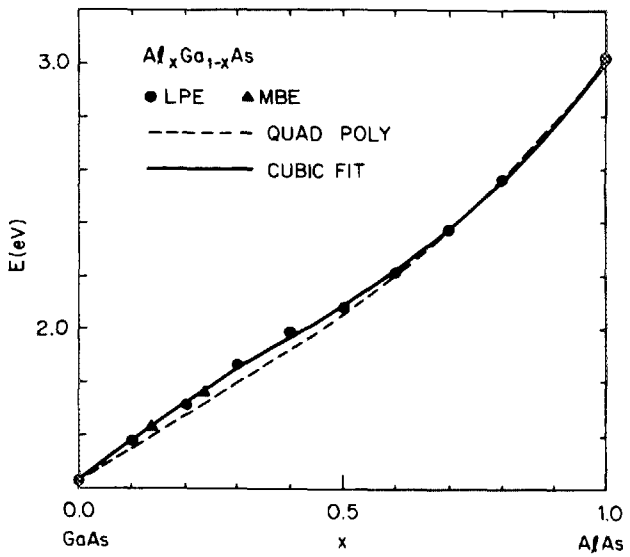

FIG. 3. Variations of the E_0 critical point threshold energies with composition, determined as described in the text. Circles: results for LPE samples. Triangles: results for MBE samples. Data for the binary endpoints were taken from Ref. 29. The dashed curve represents threshold energies calculated from the piecewise linear/quadratic expression given in Ref. 29. The solid curve is calculated from Eq. (1).

expression for $x \leqslant 0.5$, with the E_0 thresholds increasing more rapidly with target compositions for small x. The solid line is calculated from Eq. (1). It is seen that the cubic polynomial gives an excellent representation of the variation for all x, with the maximum discrepancy between target and optically determined values occurring at $x = 0.40$ where an optical composition of 0.419 is found.

The optical compositions determined by matching the measured thresholds against Eq. (1) are also given in Tables II–X. Note that the actual compositions of the samples of target compositions $x = 0.4$ and 0.5 only differ by 0.07. This small increment is also evident in the $\langle \epsilon_2 \rangle$ spectra of Fig. 2.

An important point concerning composition should be noted explicitly. The LPE target compositions themselves are referenced to standard compositions originally established by Arthur and Lepore using Auger analysis.[18] While secondary checks such as step-height differences on shadowed regions of wafers grown by molecular-beam epitaxy (MBE) have generally been consistent with the Auger analysis (see, e.g., Fig. 3), it would be useful for fundamental reasons to establish a more definitive link between the label x and the absolute Al composition to levels of precision that the optical measurements are able to achieve. The development of *in situ* growth monitoring techniques such as reflection high-energy electron diffraction (RHEED) that are capable of providing absolute Ga and Al fluences[31] offers this possibility. As more accurate methods of determining absolute composition become available, it is entirely possible that the coefficients in Eq. (1) will need to be modified. Consequently, the literal interpretation of x as absolute Al composition is perhaps premature. Fortunately, a knowledge of absolute Al concentrations is of secondary importance in optoelectronic applications, where the primary considerations are (the optically determined) refractive indices and threshold energies.

We also obtained the expression analogous to Eq. (1) for the E_1 threshold energies. The optically determined compositions were used as reference compositions for this analysis. Because the E_1 and $E_1 + \Delta_1$ critical points lie relatively close to each other (within a broadening parameter for the $x = 0.9$ sample), we investigated two methods of obtaining the E_1 threshold energies. Both were based on third derivative line shapes calculated by Fourier analysis. In the first approach, standard reciprocal-space line-shape functions[30] were fit to the Fourier coefficients themselves in the range of indices where white-noise effects were negligible. In the second approach, the Fourier coefficients were attenuated in the white-noise region by a Gaussian cutoff and were used to calculate the real-space third-derivative line shape by an inverse transformation. These real-space line shapes were then fit to standard real-space expressions[32] for the critical point line shapes. Although the two approaches are related, the information content is weighted differently in each case.[33]

Not surprisingly, the threshold values obtained were in fairly good agreement, differing by not more than 5 meV (roughly equivalent to 0.5% in x) from $x = 0.0$ to 0.6. For $x \geqslant 0.7$ the broadening parameter was so large that the real-space procedure was unable to clearly resolve the $E_1 + \Delta_1$ critical point structure from that of the E_1 transition and the

TABLE III. Pseudo-optical functions of $Al_xGa_{1-x}As$: optically determined composition $x = 0.099$.

Energy	$\langle\epsilon_1\rangle$	$\langle\epsilon_2\rangle$	$\langle n\rangle$	$\langle k\rangle$	$\langle R\rangle$	$10^{-3}\langle\alpha\rangle$ (cm^{-1})
1.500	12.758	0.000	3.572	0.000	0.316	0.00
1.600	13.401	0.434	3.661	0.059	0.326	9.62
1.700	13.521	0.600	3.678	0.082	0.328	14.06
1.800	13.798	0.738	3.716	0.099	0.332	18.13
1.900	14.237	0.962	3.775	0.127	0.338	24.54
2.000	14.563	1.305	3.820	0.171	0.343	34.63
2.100	14.981	1.540	3.876	0.199	0.349	42.29
2.200	15.471	1.864	3.940	0.237	0.356	52.74
2.300	16.067	2.216	4.018	0.276	0.364	64.29
2.400	16.796	2.627	4.111	0.320	0.373	77.73
2.500	17.662	3.225	4.220	0.382	0.384	96.83
2.600	18.732	4.023	4.353	0.462	0.397	121.79
2.700	20.080	5.196	4.518	0.575	0.413	157.38
2.800	21.744	7.213	4.725	0.763	0.433	216.63
2.900	23.411	11.184	4.968	1.126	0.461	330.89
3.000	20.038	17.765	4.838	1.836	0.483	558.25
3.100	16.095	17.384	4.460	1.949	0.469	612.35
3.200	13.306	18.598	4.253	2.187	0.475	709.22
3.300	10.072	17.026	3.864	2.203	0.458	737.04
3.400	9.205	15.494	3.690	2.100	0.441	723.61
3.500	8.846	14.619	3.601	2.030	0.430	720.13
3.600	8.699	14.060	3.552	1.979	0.423	722.19
3.700	8.690	13.736	3.532	1.945	0.419	729.33
3.800	8.809	13.609	3.537	1.924	0.417	740.99
3.900	9.028	13.692	3.566	1.920	0.419	758.97
4.000	9.342	14.017	3.618	1.937	0.423	785.31
4.100	9.734	14.664	3.697	1.983	0.431	824.19
4.200	10.146	15.766	3.801	2.074	0.444	882.91
4.300	10.364	17.571	3.922	2.240	0.464	976.34
4.400	9.851	20.145	4.017	2.507	0.489	1118.25
4.500	7.811	23.065	4.010	2.876	0.519	1311.72
4.600	4.236	24.731	3.829	3.229	0.546	1505.64
4.700	0.537	25.535	3.611	3.536	0.572	1684.43
4.800	− 4.119	25.136	3.267	3.846	0.604	1871.41
4.900	− 8.604	22.369	2.772	4.036	0.637	2004.32
5.000	− 10.991	17.583	2.207	3.983	0.662	2018.51
5.100	− 10.408	13.478	1.819	3.704	0.664	1914.68
5.200	− 9.116	11.220	1.634	3.433	0.651	1809.48
5.300	− 8.043	9.870	1.531	3.223	0.635	1731.43
5.400	− 7.227	8.928	1.459	3.059	0.621	1674.24
5.500	− 6.550	8.225	1.408	2.921	0.607	1628.38
5.600	− 5.963	7.677	1.371	2.800	0.593	1589.56
5.700	− 5.468	7.256	1.345	2.698	0.579	1558.54
5.800	− 5.032	6.937	1.330	2.608	0.565	1533.15
5.900	− 4.702	6.692	1.318	2.538	0.554	1517.71
6.000	− 4.321	6.442	1.311	2.457	0.539	1494.49

TABLE IV. Pseudo-optical functions of $Al_xGa_{1-x}As$: optically determined composition $x = 0.198$.

Energy	$\langle\epsilon_1\rangle$	$\langle\epsilon_2\rangle$	$\langle n\rangle$	$\langle k\rangle$	$\langle R\rangle$	$10^{-3}\langle\alpha\rangle$ (cm^{-1})
1.500	11.950	0.000	3.457	0.000	0.304	0.00
1.600	12.502	0.017	3.536	0.002	0.313	0.39
1.700	13.213	0.013	3.635	0.002	0.323	0.30
1.800	13.402	0.601	3.662	0.082	0.326	14.97
1.900	13.682	0.696	3.700	0.094	0.330	18.11
2.000	14.119	0.887	3.759	0.118	0.337	23.92
2.100	14.529	1.260	3.815	0.165	0.343	35.16
2.200	14.946	1.567	3.871	0.202	0.349	45.13
2.300	15.464	1.909	3.940	0.242	0.356	56.49
2.400	16.096	2.313	4.022	0.288	0.364	69.94
2.500	16.845	2.812	4.118	0.341	0.374	86.51
2.600	17.767	3.460	4.235	0.409	0.386	107.66
2.700	18.893	4.363	4.375	0.499	0.399	136.45
2.800	20.272	5.787	4.547	0.636	0.417	180.59
2.900	21.877	8.225	4.757	0.865	0.439	254.16
3.000	22.682	13.063	4.943	1.322	0.467	401.85

TABLE IV. Continued.

Energy	$\langle\epsilon_1\rangle$	$\langle\epsilon_2\rangle$	$\langle n\rangle$	$\langle k\rangle$	$\langle R\rangle$	$10^{-3}\langle\alpha\rangle$ (cm^{-1})
3.100	17.781	17.110	4.607	1.857	0.472	583.43
3.200	15.264	17.325	4.379	1.978	0.467	641.61
3.300	11.927	17.808	4.084	2.180	0.466	729.24
3.400	9.908	16.040	3.792	2.115	0.447	728.85
3.500	9.315	14.923	3.668	2.034	0.434	721.70
3.600	9.061	14.254	3.602	1.979	0.426	721.98
3.700	8.987	13.874	3.572	1.942	0.421	728.35
3.800	9.035	13.714	3.568	1.922	0.419	740.28
3.900	9.199	13.758	3.588	1.917	0.420	757.87
4.000	9.458	14.047	3.633	1.933	0.423	783.89
4.100	9.795	14.630	3.701	1.976	0.431	821.32
4.200	10.163	15.627	3.795	2.059	0.443	876.48
4.300	10.429	17.254	3.911	2.206	0.460	961.42
4.400	10.147	19.686	4.018	2.449	0.485	1092.43
4.500	8.568	22.715	4.053	2.803	0.514	1278.33
4.600	5.008	25.295	3.924	3.223	0.547	1502.86
4.700	0.459	26.010	3.638	3.575	0.576	1702.90
4.800	− 4.468	25.047	3.238	3.867	0.607	1881.50
4.900	− 8.500	21.861	2.734	3.997	0.634	1985.28
5.000	− 10.433	17.302	2.210	3.914	0.655	1983.56
5.100	− 9.895	13.595	1.860	3.654	0.654	1889.12
5.200	− 8.795	11.429	1.677	3.407	0.643	1795.77
5.300	− 7.837	10.058	1.567	3.208	0.629	1723.61
5.400	− 7.075	9.089	1.490	3.049	0.615	1668.90
5.500	− 6.426	8.346	1.433	2.912	0.602	1623.42
5.600	− 5.865	7.785	1.393	2.794	0.588	1585.91
5.700	− 5.360	7.346	1.366	2.688	0.574	1553.11
5.800	− 4.943	7.013	1.349	2.600	0.561	1528.73
5.900	− 4.611	6.776	1.339	2.531	0.549	1513.36
6.000	− 4.261	6.551	1.333	2.457	0.536	1494.40

TABLE V. Pseudo-optical functions of $Al_xGa_{1-x}As$: optically determined composition $x = 0.315$.

Energy	$\langle\epsilon_1\rangle$	$\langle\epsilon_2\rangle$	$\langle n\rangle$	$\langle k\rangle$	$\langle R\rangle$	$10^{-3}\langle\alpha\rangle$ (cm^{-1})
1.500	11.585	0.000	3.404	0.000	0.298	0.00
1.600	11.945	0.000	3.456	0.000	0.304	0.00
1.700	12.312	0.000	3.509	0.000	0.310	0.00
1.800	12.901	0.058	3.592	0.008	0.319	1.46
1.900	13.309	0.812	3.650	0.111	0.325	21.43
2.000	13.597	1.070	3.690	0.145	0.330	29.38
2.100	14.036	1.250	3.750	0.167	0.336	35.47
2.200	14.516	1.543	3.815	0.202	0.343	45.08
2.300	14.937	1.755	3.872	0.227	0.349	52.83
2.400	15.495	2.038	3.945	0.258	0.356	62.83
2.500	16.167	2.460	4.032	0.305	0.365	77.30
2.600	16.963	3.037	4.135	0.367	0.367	96.76
2.700	17.928	3.794	4.258	0.446	0.388	121.93
2.800	19.089	4.900	4.404	0.556	0.403	157.89
2.900	20.478	6.614	4.582	0.722	0.421	212.14
3.000	21.832	9.680	4.781	1.012	0.445	307.84
3.100	20.854	15.031	4.825	1.558	0.469	489.44
3.200	16.329	16.746	4.456	1.879	0.465	609.42
3.300	13.867	17.334	4.246	2.041	0.464	682.67
3.400	10.827	16.737	3.922	2.134	0.455	735.39
3.500	9.653	15.298	3.724	2.054	0.439	728.58
3.600	9.242	14.445	3.633	1.988	0.428	725.50
3.700	9.094	13.968	3.589	1.946	0.422	729.80
3.800	9.095	13.734	3.575	1.921	0.419	739.75
3.900	9.212	13.739	3.588	1.914	0.419	756.76
4.000	9.427	13.973	3.625	1.927	0.422	781.41
4.100	9.723	14.492	3.686	1.966	0.429	816.92
4.200	10.065	15.387	3.772	2.040	0.440	868.37
4.300	10.362	16.868	3.883	2.172	0.456	946.63
4.400	10.266	19.139	3.999	2.393	0.479	1067.23
4.500	9.029	22.204	4.062	2.733	0.509	1246.64
4.600	5.766	25.299	3.982	3.177	0.544	1481.12

TABLE V. Continued.

Energy	$\langle\epsilon_1\rangle$	$\langle\epsilon_2\rangle$	$\langle n\rangle$	$\langle k\rangle$	$\langle R\rangle$	$10^{-3}\langle\alpha\rangle$ (cm^{-1})
4.700	0.383	26.540	3.669	3.617	0.579	1722.91
4.800	−4.850	24.805	3.196	3.881	0.609	1888.25
4.900	−8.451	21.238	2.684	3.957	0.633	1965.08
5.000	−9.954	16.908	2.198	3.845	0.648	1948.84
5.100	−9.460	13.534	1.878	3.604	0.647	1862.86
5.200	−8.520	11.454	1.696	3.376	0.637	1779.44
5.300	−7.656	10.078	1.581	3.187	0.624	1712.04
5.400	−6.940	9.074	1.497	3.030	0.612	1658.54
5.500	−6.308	8.313	1.437	2.893	0.598	1613.01
5.600	−5.765	7.734	1.393	2.776	0.585	1575.68
5.700	−5.255	7.296	1.367	2.669	0.570	1541.99
5.800	−4.814	6.967	1.352	2.577	0.556	1514.99
5.900	−4.471	6.698	1.338	2.502	0.544	1496.52
6.000	−4.156	6.583	1.347	2.443	0.531	1486.00

TABLE VI. Pseudo-optical functions of $Al_xGa_{1-x}As$: optically determined composition $x = 0.419$.

Energy	$\langle\epsilon_1\rangle$	$\langle\epsilon_2\rangle$	$\langle n\rangle$	$\langle k\rangle$	$\langle R\rangle$	$10^{-3}\langle\alpha\rangle$ (cm^{-1})
1.500	11.160	0.000	3.341	0.000	0.291	0.00
1.600	11.412	0.000	3.378	0.000	0.295	0.00
1.700	11.709	0.000	3.422	0.000	0.300	0.00
1.800	12.106	0.000	3.479	0.000	0.306	0.00
1.900	12.669	0.018	3.559	0.003	0.315	0.49
2.000	13.423	0.431	3.664	0.059	0.326	11.91
2.100	13.578	0.735	3.686	0.100	0.329	21.21
2.200	14.022	1.003	3.747	0.134	0.335	29.86
2.300	14.562	1.357	3.820	0.178	0.343	41.40
2.400	15.015	1.700	3.881	0.219	0.350	53.29
2.500	15.582	2.120	3.957	0.268	0.358	67.88
2.600	16.279	2.581	4.047	0.319	0.367	84.03
2.700	17.103	3.202	4.154	0.385	0.378	105.49
2.800	18.100	4.037	4.280	0.472	0.391	133.82
2.900	19.273	5.279	4.430	0.596	0.406	175.12
3.000	20.591	7.236	4.605	0.786	0.425	238.89
3.100	21.579	10.694	4.778	1.119	0.448	351.61
3.200	19.457	15.439	4.706	1.640	0.466	532.03
3.300	15.873	16.459	4.401	1.870	0.461	625.45
3.400	13.237	17.043	4.172	2.042	0.460	703.85
3.500	10.814	16.101	3.887	2.071	0.448	734.87
3.600	9.940	14.982	3.736	2.005	0.435	731.61
3.700	9.622	14.365	3.668	1.958	0.427	734.32
3.800	9.516	14.059	3.640	1.931	0.424	743.92
3.900	9.549	14.005	3.640	1.924	0.423	760.47
4.000	9.696	14.201	3.667	1.936	0.425	785.08
4.100	9.942	14.663	3.719	1.971	0.431	819.31
4.200	10.229	15.482	3.794	2.040	0.441	868.66
4.300	10.519	16.846	3.897	2.161	0.456	941.92
4.400	10.530	18.973	4.014	2.363	0.477	1053.94
4.500	9.587	22.083	4.103	2.691	0.507	1227.63
4.600	6.468	25.594	4.054	3.157	0.543	1471.88
4.700	0.644	27.217	3.733	3.646	0.582	1736.73
4.800	−5.043	25.014	3.200	3.909	0.611	1901.83
4.900	−8.234	21.217	2.695	3.937	0.630	1955.15
5.000	−9.614	17.074	2.234	3.822	0.643	1936.79
5.100	−9.238	13.861	1.926	3.598	0.642	1860.13
5.200	−8.428	11.775	1.740	3.384	0.633	1783.80
5.300	−7.643	10.329	1.613	3.201	0.622	1719.58
5.400	−6.964	9.277	1.523	3.047	0.611	1667.58
5.500	−6.334	8.469	1.456	2.908	0.598	1621.01
5.600	−5.765	7.828	1.406	2.783	0.584	1579.54
5.700	−5.259	7.365	1.377	2.675	0.570	1545.40
5.800	−4.787	6.985	1.357	2.574	0.555	1513.42
5.900	−4.465	6.767	1.350	2.507	0.543	1499.39
6.000	−4.124	6.602	1.353	2.440	0.529	1483.96

TABLE VII. Pseudo-optical functions of $Al_xGa_{1-x}As$: optically determined composition $x = 0.491$.

Energy	$\langle\epsilon_1\rangle$	$\langle\epsilon_2\rangle$	$\langle n\rangle$	$\langle k\rangle$	$\langle R\rangle$	$10^{-3}\langle\alpha\rangle$ (cm^{-1})
1.500	10.780	0.000	3.283	0.000	0.284	0.00
1.600	11.080	0.000	3.329	0.000	0.289	0.00
1.700	11.344	0.000	3.368	0.000	0.294	0.00
1.800	11.676	0.000	3.417	0.000	0.299	0.01
1.900	12.089	0.000	3.477	0.000	0.306	0.02
2.000	12.659	0.016	3.558	0.002	0.315	0.46
2.100	13.423	0.647	3.665	0.088	0.327	18.80
2.200	13.639	0.985	3.696	0.133	0.330	29.72
2.300	14.115	1.234	3.761	0.164	0.337	38.25
2.400	14.685	1.571	3.838	0.205	0.345	49.79
2.500	15.176	1.914	3.903	0.245	0.352	62.12
2.600	15.797	2.331	3.985	0.292	0.361	77.07
2.700	16.525	2.900	4.081	0.355	0.371	97.24
2.800	17.411	3.596	4.195	0.429	0.382	121.66
2.900	18.445	4.623	4.328	0.534	0.396	156.98
3.000	19.629	6.132	4.483	0.684	0.413	207.96
3.100	20.801	8.624	4.654	0.926	0.433	291.11
3.200	20.801	12.735	4.753	1.340	0.455	434.48
3.300	17.419	15.823	4.525	1.748	0.461	584.80
3.400	14.745	16.502	4.294	1.922	0.458	662.21
3.500	12.074	16.529	4.034	2.049	0.454	726.82
3.600	10.534	15.419	3.822	2.017	0.440	736.17
3.700	9.992	14.670	3.724	1.969	0.431	738.60
3.800	9.771	14.294	3.680	1.942	0.427	748.01
3.900	9.737	14.190	3.671	1.933	0.425	764.12
4.000	9.821	14.346	3.688	1.945	0.427	788.49
4.100	9.995	14.768	3.730	1.980	0.433	822.67
4.200	10.237	15.540	3.798	2.046	0.442	871.00
4.300	10.502	16.815	3.894	2.159	0.456	941.02
4.400	10.547	18.847	4.009	2.351	0.476	1048.33
4.500	9.752	21.915	4.107	2.668	0.505	1216.88
4.600	6.678	25.624	4.072	3.147	0.543	1467.13
4.700	0.636	27.202	3.731	3.645	0.582	1736.48
4.800	− 5.044	24.850	3.187	3.899	0.611	1896.85
4.900	− 8.024	20.971	2.686	3.904	0.627	1938.84
5.000	− 9.278	17.038	2.250	3.787	0.639	1919.09
5.100	− 9.003	13.967	1.951	3.579	0.637	1850.21
5.200	− 8.301	11.910	1.763	3.378	0.630	1780.31
5.300	− 7.573	10.444	1.632	3.199	0.620	1718.78
5.400	− 6.923	9.330	1.532	3.045	0.609	1666.52
5.500	− 6.293	8.487	1.462	2.903	0.596	1618.56
5.600	− 5.733	7.849	1.412	2.780	0.583	1577.75
5.700	− 5.205	7.351	1.379	2.666	0.568	1540.12
5.800	− 4.755	7.018	1.364	2.572	0.553	1512.15
5.900	− 4.344	6.790	1.363	2.490	0.537	1489.38
6.000	− 3.983	6.608	1.366	2.418	0.523	1470.81

TABLE VIII. Pseudo-optical functions of $Al_xGa_{1-x}As$: optically determined composition $x = 0.590$.

Energy	$\langle\epsilon_1\rangle$	$\langle\epsilon_2\rangle$	$\langle n\rangle$	$\langle k\rangle$	$\langle R\rangle$	$10^{-3}\langle\alpha\rangle$ (cm^{-1})
1.500	10.480	0.000	3.237	0.000	0.279	0.00
1.600	10.721	0.000	3.274	0.000	0.283	0.00
1.700	10.973	0.000	3.313	0.000	0.288	0.00
1.800	11.247	0.000	3.354	0.000	0.292	0.00
1.900	11.591	0.000	3.405	0.000	0.298	0.00
2.000	12.017	0.000	3.467	0.000	0.305	0.01
2.100	12.575	0.034	3.546	0.005	0.314	1.03
2.200	13.380	0.458	3.658	0.063	0.326	13.95
2.300	13.599	0.931	3.690	0.126	0.329	29.43
2.400	14.097	1.181	3.758	0.157	0.337	38.23
2.500	14.682	1.574	3.837	0.205	0.345	51.97
2.600	15.208	2.047	3.909	0.262	0.353	69.00
2.700	15.837	2.532	3.992	0.317	0.362	86.80
2.800	16.600	3.140	4.092	0.384	0.372	108.87
2.900	17.493	3.936	4.208	0.468	0.384	137.44

TABLE VIII. Continued.

Energy	$\langle\epsilon_1\rangle$	$\langle\epsilon_2\rangle$	$\langle n\rangle$	$\langle k\rangle$	$\langle R\rangle$	$10^{-3}\langle\alpha\rangle$ (cm^{-1})
3.000	18.517	5.070	4.343	0.584	0.399	177.51
3.100	19.653	6.784	4.497	0.754	0.416	237.00
3.200	20.560	9.557	4.649	1.028	0.436	333.35
3.300	19.663	13.530	4.665	1.450	0.454	485.03
3.400	16.542	15.536	4.429	1.754	0.456	604.41
3.500	14.137	16.255	4.224	1.924	0.455	682.65
3.600	11.804	15.923	3.977	2.002	0.447	730.58
3.700	10.713	15.077	3.822	1.973	0.437	739.80
3.800	10.287	14.581	3.750	1.944	0.431	748.73
3.900	10.131	14.417	3.725	1.935	0.428	765.00
4.000	10.113	14.518	3.729	1.947	0.430	789.30
4.100	10.210	14.870	3.758	1.978	0.434	822.15
4.200	10.403	15.554	3.815	2.038	0.442	867.72
4.300	10.647	16.723	3.903	2.142	0.455	933.67
4.400	10.746	18.612	4.015	2.318	0.474	1033.77
4.500	10.194	21.592	4.127	2.616	0.502	1193.05
4.600	7.325	25.601	4.120	3.107	0.541	1448.53
4.700	1.071	27.219	3.762	3.617	0.579	1723.21
4.800	− 4.574	24.901	3.221	3.866	0.607	1880.90
4.900	− 7.553	21.268	2.740	3.881	0.623	1927.50
5.000	− 8.921	17.385	2.304	3.772	0.634	1911.84
5.100	− 8.797	14.375	2.007	3.581	0.633	1851.25
5.200	− 8.246	12.245	1.805	3.392	0.627	1787.75
5.300	− 7.589	10.682	1.661	3.217	0.619	1727.95
5.400	− 6.945	9.504	1.553	3.059	0.609	1674.41
5.500	− 6.321	8.600	1.475	2.915	0.596	1625.05
5.600	− 5.732	7.920	1.422	2.785	0.582	1580.61
5.700	− 5.195	7.413	1.389	2.669	0.567	1542.06
5.800	− 4.701	7.030	1.370	2.565	0.551	1507.87
5.900	− 4.301	6.810	1.370	2.485	0.535	1486.39
6.000	− 3.936	6.704	1.385	2.420	0.520	1471.56

TABLE IX. Pseudo-optical functions of $Al_xGa_{1-x}As$: optically determined composition $x = 0.700$.

Energy	$\langle\epsilon_1\rangle$	$\langle\epsilon_2\rangle$	$\langle n\rangle$	$\langle k\rangle$	$\langle R\rangle$	$10^{-3}\langle\alpha\rangle$ (cm^{-1})
1.500	9.940	0.000	3.153	0.000	0.269	0.00
1.600	10.161	0.000	3.188	0.000	0.273	0.00
1.700	10.398	0.000	3.225	0.000	0.277	0.00
1.800	10.636	0.000	3.261	0.000	0.282	0.00
1.900	10.928	0.000	3.306	0.000	0.287	0.00
2.000	11.294	0.000	3.361	0.000	0.293	0.00
2.100	11.728	0.001	3.425	0.000	0.300	0.03
2.200	12.252	0.003	3.500	0.000	0.309	0.09
2.300	12.924	0.016	3.595	0.002	0.319	0.51
2.400	13.653	0.513	3.696	0.069	0.330	16.89
2.500	14.012	0.969	3.746	0.129	0.335	32.78
2.600	14.582	1.408	3.823	0.184	0.344	48.54
2.700	15.200	1.918	3.906	0.245	0.353	67.19
2.800	15.806	2.446	3.987	0.307	0.361	87.05
2.900	16.538	3.058	4.084	0.374	0.371	110.04
3.000	17.393	3.857	4.196	0.460	0.383	139.75
3.100	18.378	4.965	4.325	0.574	0.397	180.35
3.200	19.450	6.576	4.471	0.735	0.413	238.51
3.300	20.334	9.049	4.615	0.980	0.432	327.96
3.400	19.925	12.658	4.665	1.357	0.450	467.51
3.500	17.454	15.104	4.502	1.678	0.456	595.12
3.600	15.128	16.217	4.319	1.877	0.457	685.06
3.700	12.864	16.355	4.103	1.993	0.453	747.43
3.800	11.550	15.837	3.947	2.006	0.446	772.81
3.900	10.928	15.538	3.868	2.009	0.442	793.97
4.000	10.620	15.516	3.836	2.023	0.442	820.09
4.100	10.487	15.765	3.835	2.055	0.444	854.10
4.200	10.502	16.330	3.868	2.111	0.450	898.74
4.300	10.595	17.349	3.932	2.206	0.461	961.51
4.400	10.632	19.053	4.028	2.365	0.478	1054.80
4.500	10.160	21.908	4.142	2.645	0.504	1206.30
4.600	7.253	26.106	4.144	3.150	0.544	1468.60

TABLE IX. Continued.

Energy	$\langle\epsilon_1\rangle$	$\langle\epsilon_2\rangle$	$\langle n\rangle$	$\langle k\rangle$	$\langle R\rangle$	$10^{-3}\langle\alpha\rangle$ (cm^{-1})
4.700	0.897	27.338	3.758	3.637	0.581	1732.65
4.800	−4.518	24.762	3.214	3.853	0.606	1874.51
4.900	−7.292	21.512	2.777	3.873	0.620	1923.76
5.000	−8.809	17.839	2.354	3.788	0.632	1919.97
5.100	−8.906	14.834	2.049	3.620	0.634	1871.32
5.200	−8.526	12.599	1.829	3.445	0.632	1815.84
5.300	−7.924	10.863	1.662	3.269	0.626	1756.01
5.400	−7.215	9.572	1.545	3.098	0.616	1695.93
5.500	−6.541	8.613	1.462	2.946	0.603	1642.26
5.600	−5.908	7.903	1.407	2.809	0.589	1594.16
5.700	−5.337	7.391	1.375	2.688	0.573	1553.18
5.800	−4.796	7.046	1.365	2.581	0.554	1517.15
5.900	−4.348	6.811	1.366	2.493	0.537	1490.74
6.000	−3.991	6.683	1.377	2.426	0.523	1475.64

TABLE X. Pseudo-optical functions of $Al_xGa_{1-x}As$: optically determined composition $x = 0.804$.

Energy	$\langle\epsilon_1\rangle$	$\langle\epsilon_2\rangle$	$\langle n\rangle$	$\langle k\rangle$	$\langle R\rangle$	$10^{-3}\langle\alpha\rangle$ (cm^{-1})
1.500	9.761	0.000	3.124	0.000	0.265	0.00
1.600	9.902	0.000	3.147	0.000	0.268	0.00
1.700	10.068	0.000	3.173	0.000	0.271	0.00
1.800	10.251	0.000	3.202	0.000	0.275	0.00
1.900	10.472	0.000	3.236	0.000	0.279	0.00
2.000	10.739	0.000	3.277	0.000	0.283	0.00
2.100	11.038	0.000	3.322	0.000	0.289	0.00
2.200	11.408	0.000	3.378	0.000	0.295	0.00
2.300	11.834	0.019	3.440	0.003	0.302	0.64
2.400	12.382	0.025	3.519	0.004	0.311	0.87
2.500	13.217	0.095	3.635	0.013	0.323	3.30
2.600	13.964	0.778	3.738	0.104	0.334	27.42
2.700	14.315	1.217	3.787	0.161	0.340	43.96
2.800	14.948	1.586	3.872	0.205	0.349	58.12
2.900	15.613	2.190	3.961	0.276	0.358	81.26
3.000	16.281	2.859	4.050	0.353	0.368	107.31
3.100	17.072	3.632	4.155	0.437	0.379	137.32
3.200	18.001	4.625	4.277	0.541	0.392	175.38
3.300	19.007	6.042	4.413	0.685	0.407	228.97
3.400	20.017	8.123	4.562	0.890	0.425	306.82
3.500	20.339	11.193	4.667	1.199	0.444	425.45
3.600	18.845	14.405	4.613	1.561	0.456	569.68
3.700	16.603	16.240	4.462	1.820	0.462	682.44
3.800	14.152	17.181	4.267	2.013	0.463	775.50
3.900	12.255	17.059	4.078	2.092	0.459	826.82
4.000	11.207	16.793	3.962	2.119	0.456	859.20
4.100	10.643	16.737	3.904	2.144	0.455	890.89
4.200	10.392	17.002	3.893	2.183	0.458	929.51
4.300	10.334	17.723	3.928	2.256	0.465	983.42
4.400	10.323	19.127	4.004	2.389	0.479	1065.33
4.500	9.941	21.704	4.112	2.639	0.503	1203.83
4.600	7.082	25.692	4.107	3.128	0.542	1458.44
4.700	1.235	26.869	3.751	3.582	0.576	1706.48
4.800	−3.720	24.345	3.233	3.765	0.597	1831.69
4.900	−6.524	21.615	2.833	3.815	0.612	1894.58
5.000	−8.274	18.256	2.426	3.763	0.625	1907.01
5.100	−8.758	15.338	2.110	3.635	0.631	1878.88
5.200	−8.628	12.909	1.857	3.475	0.633	1831.74
5.300	−8.089	10.939	1.661	3.293	0.629	1769.26
5.400	−7.300	9.489	1.528	3.104	0.619	1699.08
5.500	−6.517	8.495	1.447	2.935	0.604	1636.04
5.600	−5.837	7.808	1.399	2.792	0.587	1584.53
5.700	−5.237	7.307	1.370	2.667	0.570	1540.88
5.800	−4.722	6.931	1.354	2.560	0.552	1505.06
5.900	−4.267	6.729	1.360	2.473	0.534	1479.16
6.000	−3.931	6.589	1.368	2.409	0.520	1464.84

threshold energies determined from the real-space analysis were pulled upward. Accordingly, we use the threshold energies deduced from reciprocal-space analysis throughout. The E_1 threshold energies so obtained are shown as a function of optically determined composition in Fig. 4.

This smooth variation can also be represented by a cubic polynomial. Constraining the endpoints to the values 2.924 and 3.889 eV determined by analysis of the GaAs and capped AlAs samples, a least-squares fit to the rest of the data yields

$$E_1 = 2.924 + 0.965x + x(1-x)(-0.157 - 0.935x). \quad (2)$$

This expression is also plotted in Fig. 4. The compositions determined from Eqs. (1) and (2) agree to within 0.007 from $x = 0.0$ to 0.5 and reach a maximum discrepancy of 0.016 at $x = 0.8$, where the broadening of the E_1 critical point threshold makes it difficult to get an accurate measure of the true threshold energy. The more rapid variation of the E_0 threshold energy with x, the reduced broadening of the associated optical structure, and the greater energy separation between the primary and spin-orbit-split feature all imply that more accurate values of x are obtainable from analysis of the E_0 transition.

C. Accuracies

Although we have no means of directly assessing the absolute accuracy of the $\langle\epsilon\rangle$ data, we estimate from Kramers–Kronig consistency that the data for $x \leqslant 0.5$ are probably accurate to within 2% of the maximum value of ϵ for any given spectrum, and to within 5% for compositions $x \geqslant 0.6$. Instrument uncertainties are estimated to contribute less than 1%, since data taken on different rotating-analyzer ellipsometers now generally show mutual agreement to within this amount.[34,35]

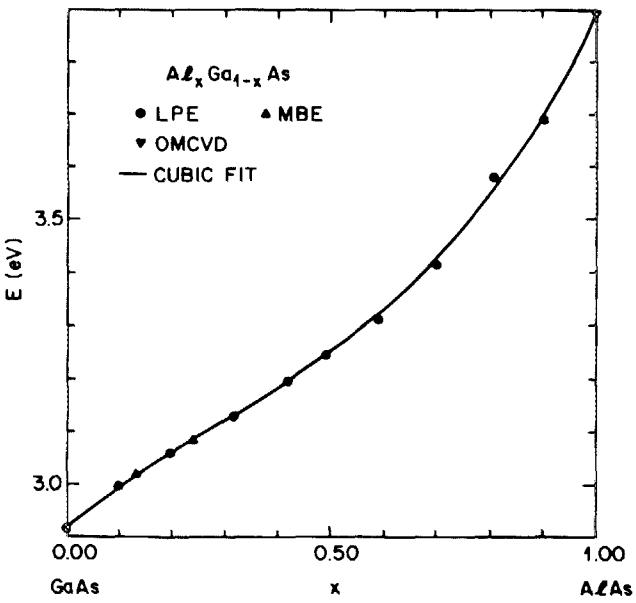

FIG. 4. As Fig. 3, but for the E_1 threshold. The value for AlAs was determined from the OMCVD sample assuming coverage by 40 Å of GaAs. The points are located according to the optically determined compositions calculated from the E_0 threshold data and Eq. (1).

However, we can make more systematic estimates of the accuracy by examining trends in the data as a function of optically determined composition. Figures 5 and 6 show the values of $\langle\epsilon_1\rangle$ at 1.5 eV and the height of the E_2 peak in $\langle\epsilon_2\rangle$ as a function of the optically determined composition. The former quantity is relatively independent of surface effects and is a measure of various sample-to-sample inaccuracies, while the latter is primarily a measure of relative surface quality and the sample-to-sample reproducibility of the surface preparation procedures. Data for the MBE samples are shown as triangles. Two points are shown for GaAs, one corresponding to the data obtained on the LPE sample grown as part of the set, and the second to the bulk sample whose data were reported in Ref. 22. The two points for GaAs are so close to each other in Fig. 5 that they cannot be distinguished. Also in Fig. 5, the data for the sample of target composition $x = 0.80$ prior to the Kramers–Kronig self-consistency correction peculiar to this sample, as discussed above, are represented by the asterisk.

In Fig. 6, the datum for the OMCVD sample is calculated assuming a 40-Å cap layer of GaAs. The AlAs thickness variation prevented the determination of the cap layer thickness by standard methods and the detailed analysis of the data in the spectral range near and below the E_0 transition. However, the 40-Å value is consistent with that estimated from growth conditions, with the approach of ϵ_2 to zero in the vicinity of the E_0 threshold, and with the linear extrapolation of E_2 peak heights for the samples with $x \leqslant 0.5$ as seen in Fig. 6. Even if the cap layer were ignored completely, a lower bound of 27.3 is established for the E_2 peak height in AlAs. Consequently, at worst, the use of GaAs as a protective cap for AlAs affects the AlAs E_2 peak height by no more than 10% because the dielectric responses of GaAs and AlAs at this wavelength are so similar.

While the exact functional forms that the values shown in Figs. 5 and 6 should take are matters of speculation, it is clear that the scatter in these data for $x \leqslant 0.5$ does not exceed ± 0.2. This is less than 1% of the peak values of either the

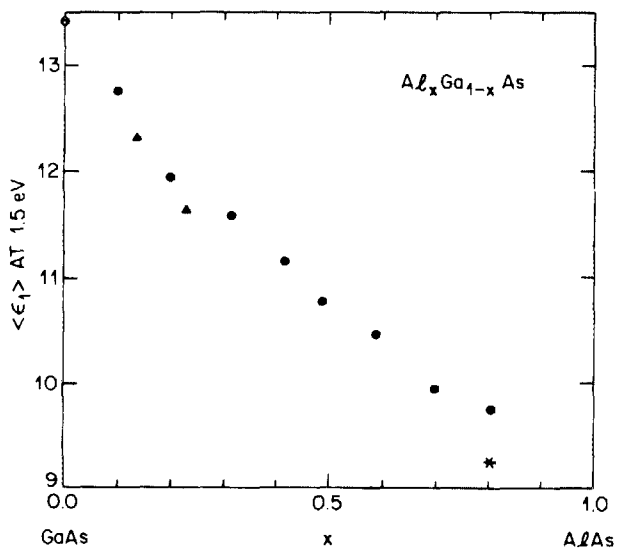

FIG. 5. Variation of the value of $\langle\epsilon_1\rangle$ at 1.5 eV as a function of optically determined composition, illustrating typical levels of scatter in the data. The asterisk is described in the text.

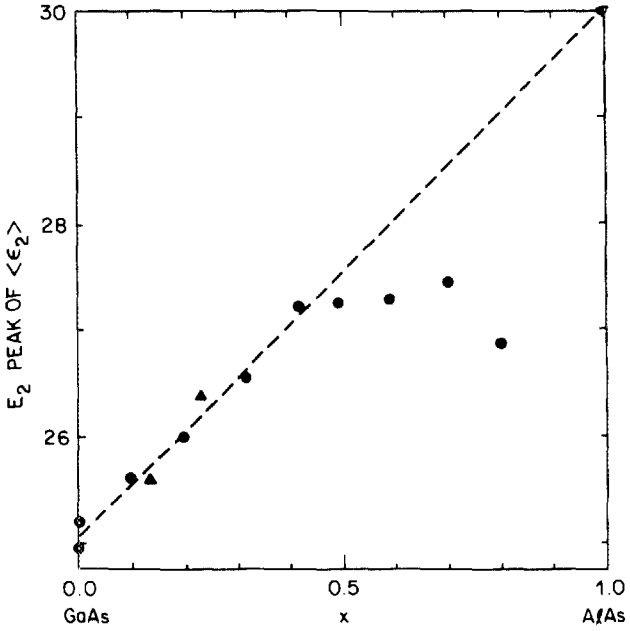

FIG. 6. As Fig. 5, but for the E_2 peak in $\langle\epsilon_2\rangle$. The datum for AlAs was evaluated assuming that the thickness of the protective GaAs cap layer was 40 Å, as discussed in the text.

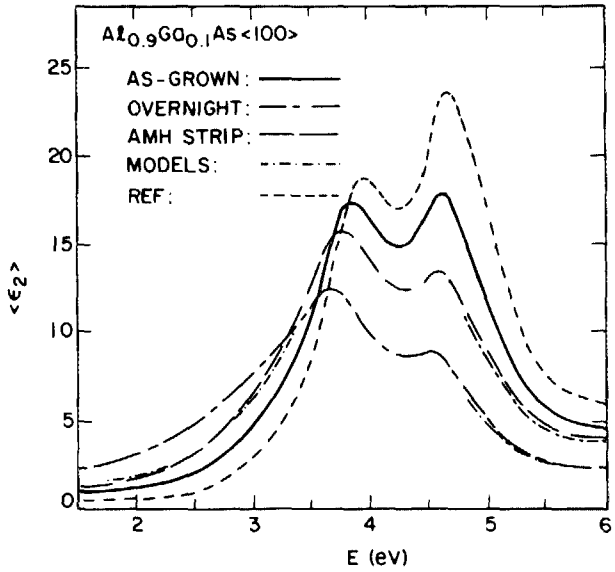

FIG. 7. $\langle\epsilon_2\rangle$ spectra for a sample with target composition $x = 0.90$ after various surface treatments. Solid line: as-grown surface, 2-h delay before measurement. Dash-dot line: as-grown surface, 20-h delay before measurement. Long dashed line: after stripping previous surface with 1:1 $NH_4OH:H_2O$. Short dashed line: reference spectrum. The results of the model calculations described in the text can be seen as dot-dash segments.

$\langle\epsilon_1\rangle$ or $\langle\epsilon_2\rangle$ spectra themselves. For higher values of x the peak heights show systematic variations indicating incomplete removal of oxide overlayers. The fact that overlayers cannot be completely removed by chemical means for samples with high Al concentrations is not surprising, as will be shown more directly in the following section.

D. Oxidation of a sample with $x = 0.90$

Samples with target compositions $x = 0.90$ and 1.00 (AlAs) were so reactive that the accuracy level to which the previous data were obtained could not even be approached by chemical cleaning. However, the oxidation of a sample with target composition $x = 0.90$ was studied to determine how high-Al content alloys degrade, as the results obviously have some bearing on degradation mechanisms in alloys with lower Al content as well.

Figure 7 shows $\langle\epsilon\rangle$ data for the $Al_{0.90}Ga_{0.10}As$ sample 2 h after growth, 20 h after growth, and after stripping with 1:1 $NH_4OH:H_2O$. A "reference" spectrum is also shown, obtained by following the preparation procedure described in Table I for the sample with $x = 0.80$. We emphasize that the "reference" spectrum is already considerably distorted by a surface film, as evidenced by the nonzero value of $\langle\epsilon_2\rangle$ at low energies and the relatively low value of the E_2 peak in $\langle\epsilon_2\rangle$ with respect to those shown in Fig. 6. Both discrepancies could be eliminated to good accuracy by mathematically removing a 15-Å layer of SiO_2, although the procedure can be justified on physical grounds only if one assumes that all oxides have essentially the same effect on $\langle\epsilon\rangle$. The spectra for 2 and 20 h after growth show the effect of a thick overlayer which, by the reduction in amplitude of the E_1 peak, must be absorbing in this spectral region.

These spectra were fit by a four-phase model consisting of a "substrate" given by the dashed curve in Fig. 7, a physically mixed region consisting of the "substrate" and Al_2O_3, a pure Al_2O_3 oxide, and the ambient. The optical functions[36] of Al_2O_3 were used for simplicity, since the actual oxide is probably a mixture of Al_2O_3, As_2O_3, and some Ga_2O_3, whose optical properties are not known. The results were as follows. For 2-h air exposure the mixed phase consisted of 61% "substrate" and 39% oxide and was 13 Å thick, while the oxide was 9 Å thick. For 20-h air exposure the mixed phase consisted of 70% "substrate" and 30% oxide and was 59 Å thick, while the oxide was also 59 Å thick. After stripping with 1:1 $NH_4OH:H_2O$ the mixed phase consisted of 30% "substrate" and was 30 Å thick, while the oxide was 15 Å thick. The presence of a thick physically mixed substrate–oxide region shows that oxidation does not proceed uniformly, but irregularly via a penetration mechanism presumably following the spatial distribution of the more reactive Al species.

E. Interpolation

The spectral presented here have one disadvantage with respect to optical modeling: they are not expressed as continuous analytic functions of the composition x. The next step is clearly to apply the harmonic oscillator analysis (HOA) procedure of Erman[37] to represent these data in a more convenient form. However, for many cases of interest, only the limited spectral range about E_1 is desired. In applications of this type we have simulated a continuous compositional variation over narrow energy ranges by taking the appropriately weighted average of the two spectra closest in composition after their energy scales have been appropriately shifted to bring the nearest critical point energies into coincidence. The assumption, which is at least partially justified by Figs. 1, 2, 5, and 6, is that the amplitudes vary relatively slowly with composition, with the primary spectral variation being due to the critical point threshold energies.

IV. CONCLUSION

In this work, we have presented pseudodielectric function data for a series of $Al_x Ga_{1-x} As$ samples of compositions in the range $x = 0.00$–0.80. The data are accurate to within current capabilities, and are probably accurate to within 2% of peak values for $x \leqslant 0.5$, which is the useful compositional range for technological applications.

For most compositions, these data are presently the only complete set available. However, we do not believe that they will necessarily be the final set since certain areas for improvement can be identified. First, the surfaces were prepared by chemical treatment, which by Fig. 6 cannot remove surface overlayers on samples with high Al concentrations. Measurements performed on freshly prepared samples within the growth chamber will be necessary to overcome this limitation. Alternatively, measurements could also be made on GaAs-capped samples provided that the thickness of the underlying alloy is uniform to within a few Å.

Second, the nominal compositions are all referenced to relatively early Auger work by Arthur and Lepore.[18] The development of *in situ* techniques such as RHEED that have the capability of providing absolute MBE flux rates[31] offers the possibility of compositional accuracies to the levels of precision that optical techniques are currently able to achieve. Thus, we expect the compositional data ultimately to be calibrated in absolute terms. Fortunately, absolute Al concentrations are of secondary importance in optoelectronic applications, where the primary considerations are (the optically determined) refractive indices and threshold energies.

Finally, the adaptation of the harmonic oscillator approximation of Erman[37] to these data will allow them to be expressed in analytic form for direct and more convenient use in optical modeling. These aspects are all expected to be subjects of further work.

Note added in proof. Miller *et al.*[38] recently correlated measured room-temperature photoluminescence peak energies E_p with measured electron probe microanalysis compositions x for $Al_x Ga_{1-x} As$ alloys of $x = 0$–0.45. Assuming $E_p = E_0$, compositions obtained from their expression agree to within statistical uncertainty to those obtained from Eq. (1) over the entire common range, differing by less than 0.010 for $0 \leqslant x \leqslant 0.05$ and $0.35 \leqslant x \leqslant 0.45$ and reaching a maximum difference of 0.016 at $x \cong 0.15$. While this consistency represents an encouraging improvement, absolute compositional calibrations are still desirable.

ACKNOWLEDGMENTS

We thank A. C. Gossard and W. Wiegmann for permission to cite the results of the analysis of the two MBE samples.

[1] A. C. Gossard, W. Brown, C. L. Allyn, and W. Wiegmann, J. Vac. Sci. Technol. **20**, 694 (1982).
[2] F. Capasso, J. Vac. Sci. Technol. B **1**, 457 (1983).
[3] R. C. Miller, A. C. Gossard, D. A. Kleinman, and O. Munteanu, Phys. Rev. B **29**, 3740 (1984).
[4] F. Capasso, K. Mohammed, and A. Y. Cho, J. Vac. Sci. Technol. B **3**, 1245 (1985).
[5] R. Bhat, W. K. Chen, A. Kastalsky, M. A. Koza, and P. S. Davisson, Appl. Phys. Lett. **47**, 1344 (1985).
[6] G. Laurence, F. Hottier, and J. Hallais, Rev. Phys. Appl. **16**, 579 (1981).
[7] M. Erman, J. B. Theeten, N. Vodjdani, and Y. Demay, J. Vac. Sci. Technol. B **1**, 328 (1983).
[8] M. Erman and P. J. Frijlink, Appl. Phys. Lett. **43**, 285 (1983).
[9] D. E. Aspnes and S. M. Kelso, Soc. Photo-Opt. Eng. Proc. **452**, 79 (1983).
[10] M. Erman, J. B. Theeten, P. Frijlink, S. Gaillard, F. J. Hia, and C. Alibert, J. Appl. Phys. **56**, 3241 (1984).
[11] R. A. Höpfel, J. Shah, A. C. Gossard, and W. Wiegmann, Appl. Phys. Lett. **47**, 163 (1985).
[12] O. J. Glembocki, B. V. Shanabrook, N. Bottka, W. T. Beard, and J. Comas, Appl. Phys. Lett. **46**, 970 (1985).
[13] H. C. Casey, D. D. Sell, and M. B. Panish, Appl. Phys. Lett. **24**, 63 (1974).
[14] B. Monemar, K. K. Shih, and G. D. Pettit, J. Appl. Phys. **47**, 2604 (1976).
[15] E. Kuphal and H. W. Dinges, J. Appl. Phys. **50**, 4196 (1979).
[16] W. Both and B. Geselle, Cryst. Res. Technol. **17**, K30 (1982).
[17] M. B. Panish and M. Ilegems, "Phase Equilibria in Ternary III–V Systems," in *Progress in Solid State Chemistry*, edited by H. Reiss and W. O. McCaldin (Pergamon, New York, 1972), Vol. 7, p. 39.
[18] J. R. Arthur and J. J. LePore, J. Vac. Sci. Technol. **14**, 979 (1977).
[19] D. E. Aspnes and A. A. Studna, Appl. Opt. **14**, 220 (1975); Rev. Sci. Instrum. **49**, 291 (1978).
[20] D. E. Aspnes, J. Opt. Soc. Am. **64**, 812 (1974).
[21] D. E. Aspnes and A. A. Studna, Appl. Phys. Lett. **39**, 316 (1981).
[22] D. E. Aspnes and A. A. Studna, Phys. Rev. B **27**, 985 (1983).
[23] D. E. Aspnes, J. Vac. Sci. Technol. **17**, 1057 (1980).
[24] D. E. Aspnes and A. A. Studna, Appl. Phys. Lett. **46**, 1071 (1985).
[25] R. M. A. Azzam and N. M. Bashara, *Ellipsometry and Polarized Light* (North-Holland, Amsterdam, 1977).
[26] D. E. Aspnes, in *Handbook on Optical Constants of Semiconductors*, edited by E. Palik (Academic, New York, 1985), pp. 89–112.
[27] For each of the alloys, the semiconductors studied in Ref. 22, and selected other materials, the data are also available as 250 pseudodielectric function values equally spaced in energy from 1.5 to 6.0 eV. They can be obtained by sending the first author a 5¼-in. floppy disk initialized for the Digital Equipment Corporation RT-11 operating system and RX-50 disk drive.
[28] P. M. Petroff and R. A. Logan, J. Vac. Sci. Technol. **17**, 1113 (1980).
[29] H. C. Casey, Jr., and M. B. Panish, *Heterostructure Lasers*, Part A (Academic, New York, 1978), pp. 192–3.
[30] D. E. Aspnes, Surf. Sci. **135**, 284 (1983).
[31] T. Sakamoto, H. Funabashi, K. Ohta, T. Nakagawa, N. J. Kawai, T. Kojima, and Y. Bando, Superlattices and Microstructures **1**, 347 (1985).
[32] D. E. Aspnes, Surf. Sci. **37**, 418 (1973).
[33] D. E. Aspnes and H. Arwin, J. Opt. Soc. Am. **73**, 1759 (1983).
[34] L. Viña, C. Umbach, M. Cardona, and L. Vodopyanov, Phys. Rev. B **29**, 6752 (1984).
[35] P. G. Snyder, M. C. Rost, G. H. Bu-Abbud, J. Oh, J. A. Woollam, D. Poker, D. E. Aspnes, D. Ingram, and P. Pronko, J. Appl. Phys. (in press).
[36] I. H. Malitson, J. Opt. Soc. Am. **52**, 1377 (1962).
[37] M. Erman, J. B. Theeten, P. Chambon, S. M. Kelso, and D. E. Aspnes, J. Appl. Phys. **56**, 2664 (1984).
[38] N. C. Miller, S. Zemon, G. P. Weber, and W. Powazinik, J. Appl. Phys. **57**, 512 (1985).